Numerical study of hydrodynamic and salinity transport process in Pink Beach wetlands of Liao River Estuary, China

Huiting Qiao[1], Mingliang Zhang[1*], Hengzhi Jiang[2], Tianping Xu[1] and Hongxing Zhang[1]

[1] School of Ocean Science and Environment, Dalian Ocean University, Dalian, Liaoning, 116023, China;

[2] National Marine Environment Monitoring Center, Dalian, Liaoning, 116023, China

Correspondence: Mingliang Zhang (zhmliang_mail@126.com)

Abstract. The interaction study of vegetation with the flow environment is essential for the determination of the bank protection, morphological characteristics and ecological conditions for the wetlands. This paper uses MIKE 21 hydrodynamic and salinity model to simulate the hydrodynamic characteristics and salinity transport process in Pink Beach wetlands of Liao River estuary. The effect of wetland plants on tidal flow in areas of wetland waters is represented by a varying Manning's coefficient in the bottom friction term. Acquisition of vegetation distribution is based on Landsat TM satellites through remote sensing techniques. Detailed comparisons between field observation and simulated results of water depth, salinity and tidal currents are presented in vegetated domain of Pink Beach. Satisfactory results are obtained in simulating both flow characteristics and salinity concentration with or without vegetation. A numerical experiment was conducted based on variations of vegetation densities, and compared with the tidal currents in the non-vegetated area. Computed current speed decreased remarkably with an increase in the vegetation density. The impact of vegetation on water depth and salinity is simulated, and the finding reveals that the wetland vegetation has insignificant effect on the water depth and salinity in wetland domain. Several stations from upstream to downstream in the Pink Beach are selected to estimate the longitudinal variation of salinity under different river runoff and the results show that the salinity concentration decreases with an increase of river runoff. This study can help to increase understanding of the favourable salinity conditions for the

special vegetation growth in the Pink Beach wetlands of Liao River estuary. The results provide crucial guidance for related interaction studies among vegetation, flow and salinity in other wetland waters.

1 Introduction

Wetland is a transitional zone between terrestrial ecosystems and aquatic ecosystems, and has a variety of unique functions, providing large amounts of food, raw materials and water resources for humans, maintaining the ecological balance, biodiversity and rare species resources. The scope for aquatic plants in coastal protection from extreme events has become a recurring question along with the viability assessment of ecosystem-based management approaches (Barbier et al., 2008; Temmerman et al., 2013). Coastal wetlands are mainly distributed in coastal areas in China within eleven areas (Hebei, Liaoning, Shandong, Jiangsu, Zhejiang, Fujian, Guangdong, Hainan, Taiwan, Tianjin and Guangxi). Coastal wetlands cover an area of 5.7959×10^6 ha, accounting for 10.85% of the total area of wetlands in China, there are 12 types of coastal wetland plants (Jiang et al., 2015). Liao River estuary wetland is located in Panjin City, Liaoning Province, China, with a total wetland area of about 451300.5 ha (Zhang et al., 2009). The main wetland vegetations include *Phragmites communis* and *Suaeda heteroptera*, which lie in the inter-tidal zone of the Liao River estuary. *Suaeda heteroptera* is a dominant species in the wetland of Liao River estuary and a typical saline-alkaline indicator plant, most of which are distributed in coastal tidal flats, forming a rare natural landscape “pink beach” in China (Fig. 1). The main factor limiting the growth of the *Suaeda heteroptera* is the water salinity and the most suitable salinity for its growth is about 15 psu (practical salinity units): lower than or higher than 15 psu, the *Suaeda heteroptera* will be degraded or inhibited. The salinity and water content are the main limiting factors for the growth of *Phragmites communis*, especially the salinity, and high salinity of the soil can inhibit the growth of *Phragmites communis*. Therefore, when the runoff of the river is large, the *Phragmites communis* will invade the growth area of the *Suaeda heteroptera*, resulting in community succession.

Figure 1. *Suaeda heteroptera* in Liao River estuary wetland

Recently, wetland ecosystems have been severely damaged and degenerated through disproportionate consumption of wetland ecological resources, which in turn has resulted in serious declines in biodiversity and biological resources. A variety of studies on hydrodynamics in estuarine wetlands have been conducted, which mainly include the following aspects: interaction between flow and vegetation, pollutant transport in wetland and vegetation resistance experiment. The relevant research is mainly to study the resistance coefficient of water flow when plants exist; most of them are characterized by Manning coefficient of water resistance (Ree et al., 1958; Chow et al., 1959). In addition, some scholars have studied the influence of plants on the structure of water flow, such as changes to flow turbulence intensity and boundary shear force (Ikeda et al., 1996). Considering the height and bending degree of the willow species by water flooding, the vegetation resistance was introduced into the Navier-Stokes equation and numerical simulation of the three-dimensional flow field of the river and the floodplain wetland was carried out (Wilson, 2006). Taking the reed community as the research object, Shi

et al. (2001) carried out an experiment to investigate the water resistance of non-submerged reeds and the relationship between the density and the resistance of reeds. Based on velocities in laboratory experiments for different water depths, discharges and aquatic vegetation densities, analyses were made for the resistance coefficient of vegetation (Li et al., 2004).

Saint-Venant equation and Nuding model were combined to simulate the steady-state and unsteady flow in the presence of vegetation in a channel and to analyse the effects of vegetation cover, beach slope and width on the cross-section of a river (Helmiö, 2005). A two-dimensional nonlinear hydrodynamic model (WETFLOW model) was established for wetlands with gentle slopes and the one-dimensional and two-dimensional forms were validated by using indoor model and field pond wetland (Feng et al., 1997). The coupled SWIFT2D surface water and SEAWAT groundwater migration model were used to simulate the hydrological processes and salt exchange of surface water and groundwater in estuaries and adjacent coastal wetlands (Christian et al., 2005). The two-dimensional numerical model was used to test the different flow conditions of ZhaLong wetland, and the effect of reed wetland in the process of storage and detention was comprehensively evaluated (Gu et al., 2006). The 2D k-ε turbulence hydrodynamic model for a curved open channel flow in curvilinear coordinates has been set up to simulate the hydrodynamic behavior of turbulent flow in open channel partially covered with vegetation; the effect of vegetation on flow was treated both by drag force method and equivalent resistance coefficient method (Zhang et al., 2013). Besides, some tidal flat wetland simulations have been carried out. The Delft3D model was used to investigate the wetland impact on tidal movement and turbulence for the semi-enclosed Breton Sound (BS) estuary in coastal Louisiana (Hu et al., 2014). The Telemac Modelling System (TMS) was applied to the development of a hydro-environmental model of the Severn Estuary and Bristol Channel to study microbial tracer transport processes due to mortality or interaction with the sediments, vegetation or some other water quality constituent (Abu-Bakar et al., 2017). Stark et al. (2017) established a depth-averaged hydrodynamic model (TELEMAC-2D) to assess the tidal hydrodynamics in marsh channels of the Saeftinghe in the Netherlands during different stages of marsh development. Development towards a marsh system with a

channel network and a vegetated platform is strongly influenced by the pioneer vegetation. Christiansen et al. (2000) introduced the physical processes of controlling mineral sediment deposition on a meso-tidal salt marsh surface on the Atlantic Coast of Virginia; wetland plants patches reduce flow velocities locally and enhance sedimentation inside the patches. Bouma et al. (2005) collected a series of hydrodynamic data from the Scheldt Estuary beaches and swamps, and found that there was a clear linear relationship between the tidal amplitude and the maximum velocity in flats and vegetation area, meanwhile, the flow rate was obviously lower in vegetation area. Su et al. (2013) developed a model known as mangrove-hardwood hammock model, and simulated the evolution of vegetation succession along with changing groundwater salinity. The results demonstrate the impact of sea level rise on coastal vegetation and groundwater salinity. Lapetina et al. (2014) developed a 3D storm surge model with plants effect; the model is applicable to assess the feasibility of future wetland restoration projects. Regarding study of salt intrusion in wetland, Andrew et al. (2017) constructed a 3-D hydrodynamic model of San Francisco Estuary and found estuarine circulation was strongest during neap tides and unsteady salt intrusion was strongest during spring tides. A three-dimensional hydrodynamic model (CH3D) was used to investigate the impact of physical alteration on salinity in Caloosahatchee Estuary (Sun et al., 2016).

In general, the majority of studies have focused on the effects of vegetation on fluid movement in flume experiments, few detailed field observations or salinity simulations exist in mudflat–salt marsh ecosystems, especially in typical wetland plant of Liao River estuary. Research on the salinity response to river discharge in wetland waters is not yet systematically assessed.

In this study, a 2-D hydrodynamic and salinity model is used to simulate flow patterns and salinity distribution in wetland waters of Liao River estuary. The resistance caused by vegetation is represented by the varying Manning coefficient. This study adopts remote sensing techniques to obtain the spatial distribution of two types aquatic plants in Pink Beach. The

numerical model is calibrated and validated against field measurement data; the variation of salinity in vegetated domain of the Pink Beach wetland is obtained under different runoff conditions.

2 Numerical Models

The MIKE 21 model, one of the most widely used hydrodynamic models, was developed by Danish Hydraulic Institute (DHI) and has been widely used in domestic and overseas research (Wang et al., 2013). The model is based on the cell-centered finite volume method implemented on an unstructured flexible mesh. It includes hydrodynamic, transport, ecological module/oil spill, particle tracking, mud transport, sand transport, and inland flooding modules (Cox, 2003).

2.1 Hydrodynamic module

The Hydrodynamic module is based on numerical solution of the depth-integrated incompressible flow Reynolds-averaged mass conservation and momentum equations (William, 1979). The governing equations include:

Continuity conservation:

$$\frac{\partial h}{\partial t}+\frac{\partial h\bar{u}}{\partial x}+\frac{\partial h\bar{v}}{\partial y}=hS \tag{1}$$

Momentum equations:

$$\frac{\partial h\bar{u}}{\partial t}+\frac{\partial h\bar{u}^{2}}{\partial x}+\frac{\partial h\overline{vu}}{\partial y}=f\bar{v}h-gh\frac{\partial \eta}{\partial x}-\frac{h}{\rho_0}\frac{\partial P_a}{\partial x}-\frac{gh^2}{\rho_0}\frac{\partial \rho}{\partial x}+\frac{\tau_{sx}}{\rho_0}-\frac{\tau_{bx}}{\rho_0}+\frac{\partial}{\partial x}\left(hT_{xx}\right)+\frac{\partial}{\partial y}\left(hT_{xy}\right)+hu_sS \tag{2}$$

$$\frac{\partial h\bar{v}}{\partial t}+\frac{\partial h\bar{v}^{2}}{\partial x}+\frac{\partial h\overline{uv}}{\partial y}=-f\bar{u}h-gh\frac{\partial \eta}{\partial y}-\frac{h}{\rho_0}\frac{\partial P_a}{\partial y}-\frac{gh^2}{\rho_0}\frac{\partial \rho}{\partial y}+\frac{\tau_{sy}}{\rho_0}-\frac{\tau_{by}}{\rho_0}+\frac{\partial}{\partial x}\left(hT_{yx}\right)+\frac{\partial}{\partial y}\left(hT_{yy}\right)+hv_sS \tag{3}$$

where x and y are the Cartesian coordinates; $h = \eta + d$ is the total water depth; t is time; η is water surface elevation; d is the still water depth; ρ is density of water; ρ_0 is a ratio of water density to air density; g is acceleration due to gravity; $\bar{u}$ and $\bar{v}$ are the depth-averaged velocity components in x and y directions; f is the Coriolis parameter; S is the magnitude of the discharge due to point sources; p_a is the atmospheric pressure; (u_s, v_s) is the velocity components in x and y directions for point sources; T_{xx}, T_{xy}, T_{yx} and T_{yy} are the components of the effective shear stress due to turbulence and visous effects; (τ_{sx}, τ_{sy}) and (τ_{bx}, τ_{by}) are the x and y components of the surface wind and bottom stresses. $\frac{\tau_b}{\rho_0} = c_f \vec{u}_b \left|\vec{u}_b\right|$, $\vec{u}_b = (u_b, v_b)$ is the depth-averaged velocity for two-dimensional calculations, $c_f = \frac{g}{(Mh^{1/6})^2}$, $M = 25.4/k_s^{\frac{1}{6}}$, M is the Manning coefficient for the bed roughness in MIKE 21 model, k_s is roughness height (DHI, 2007).

2.2 Salinity module

The fundamental salinity equation is:

$$\frac{\partial h\bar{s}}{\partial t} + \frac{\partial h\bar{u}\bar{s}}{\partial x} + \frac{\partial h\bar{v}\bar{s}}{\partial y} = hF_s + hs_s S \tag{4}$$

where $\bar{s}$ is the depth-averaged salinity under average water depth, s_s is the salinity of the source, F_s is the horizontal diffusion terms of the salinity.

3 Numerical simulation and validation

3.1 Description of the study domain

The Liao River is one of the largest seven rivers in China and is located in the north of the Liaodong Bay, China. This estuary is a crucial ecological economic zone, which plays an important role for the comprehensive development and

utilization of marine industry in China. The Liao River estuary includes Daliao River and Liao River (Li et al., 2017). The Pink Beach of Liao River Delta is a marsh wetland covered with *Phragmites communis* and *Suaeda heteroptera*; it has been listed as the largest reed wetland and the second largest marshes in the world. It provides an important habitat for a variety of marine wildlife, especially for some endangered species, such as *Phoca largha*, *Larus saundersi* and *Grus japonensis*. However, over the past decade, the Pink Beach wetland has been significantly degraded and *Suaeda heteroptera* community decreased by the global warming, environmental pollution and other natural or human factors. Some studies on tidal flat wetland have shown that the growth of marsh plant community is associated with a limited range of salinity (Zhang, et al, 2009). However, due to the lack of quantitative salinity observations, the impact of actual salinity on vegetation growth is still unknown for the Pink Beach wetland of Liao River.

Study domain is located at the north of Liaodong Bay, extending from 40.3032 ° to 40.7105 ° North and 121.0294 ° to 122.0312 ° East (Fig. 2). An unstructured triangular mesh of Liao River estuary (Fig. 3) was generated using bathymetry data by SMS (Surface Water Model System) software. The number of cells was 18108 with 9599 nodes in the computational domain. From the upper reaches of the river to the central part of the domain, i.e. at the Pink Beach wetland, which is the focus of the present study, we use finer grid resolutions, as small as 98 m. Model grid size increases gradually away from the flats and estuarine deltas, and maximum grid spacing in the open sea is 2460 m. Then the topographic map was obtained through terrain interpolation (Fig. 3).

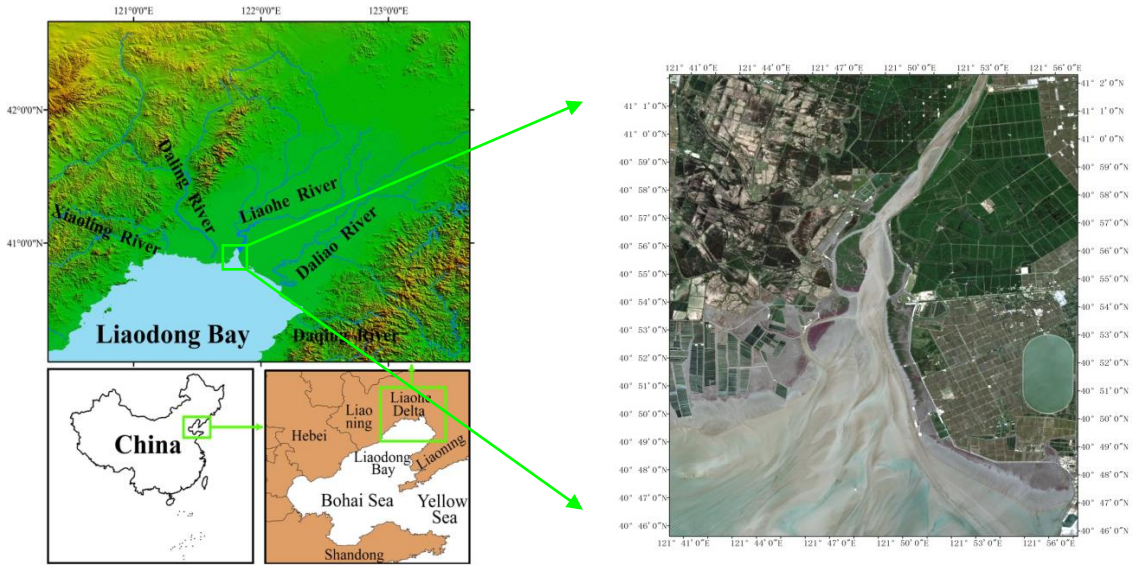

Figure 2. The geographical location (Wang et al., 2017) and satellite image of the Liao River Estuary

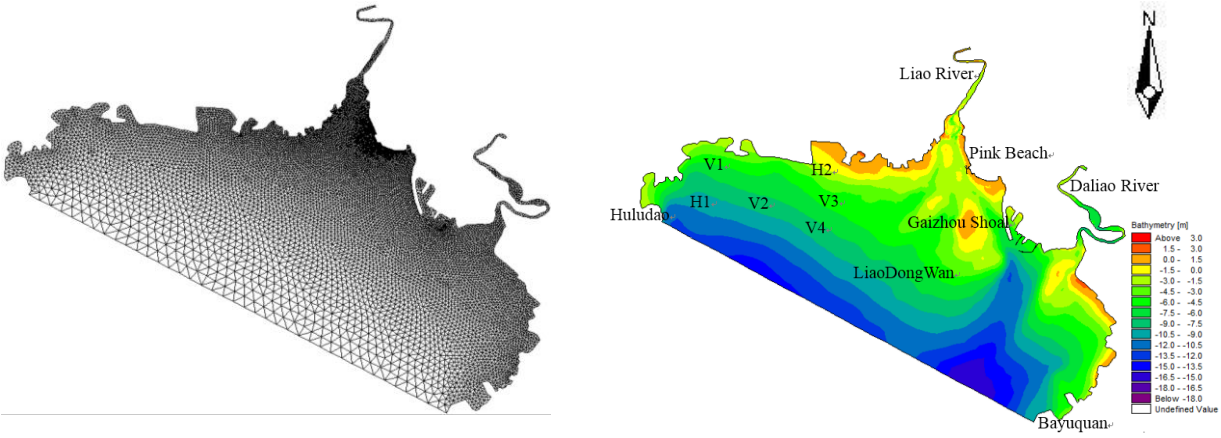

Figure 3. Model grids, bathymetry and the validation points

To proceed with the numerical simulations, the equations of hydrodynamics require appropriate boundary and initial conditions. A total of three open boundaries and the solid boundary are established. The model was forced at the open boundary, from Huludao to Bayuquan, by a time series of tidal elevations from the TMD (Tide Model Driver) (Padman L.,

2005). Two flow boundaries in the north of area are controlled by the discharge. The solid boundary is treated as impermeable with no slip. The salinity data of the open boundary and river discharge are set to 32.8 and 2 psu in this model. The initial water level and salinity are 0 m and 32 psu, respectively.

3.2 Simulation of tidal currents and salinity

Simulation is carried out to verify the accuracy of the model. Simulations with a larger time step caused systematic violations of the Courant Number (i.e., CN > 1), whereas smaller time steps significantly increased the computational time. The model is an explicit format with a maximum time step of half an hour, and it automatically adjusts the time step according to the CFL (Courant-Friedrichs-Lewy) conditions during the calculation. The parameter M represents Manning's coefficient for bed roughness and is 80 $m^{1/3}s^{-1}$ in this study. Hydrodynamic model was run for the period May 1, 2013, to May 31, 2014. A model spin-up period of a year was performed to achieve stabilization from May 1, 2013, to May 1, 2014, and tidal water levels, tidal currents, and salinity throughout the water column were used as calibration parameters over the period May 21, 2014, to May 30, 2014. There was a neap tide between May 21 and May 22, 2014, and a spring tide between May 29 and May 30, 2014. There were two tide level monitoring stations (H1 and H2) and four tidal current monitoring stations (V1, V2, V3 and V4) (Tab. 1 and Fig. 3).

Table 1. The coordinate of monitoring stations

Station	Latitude	Longitude
H1	40°47.616'	121°04.833'
H2	40°50.151′	121°23.696′
V1	40°49.226′	121°08.471′
V2	40°48.660′	121°15.278′
V3	40°48.400′	121°24.349′
V4	40°43.839′	121°23.522′

The water levels and the tidal currents in the study domain are calculated, the results of numerical simulation were compared with measured data in terms of water levels and tidal currents, as shown in Fig.4, Fig.5 and Fig.6. The model matched the timing of observed tidal water levels at two locations (Fig. 4), with no detectable phase shift in water levels, but the model slightly underestimates the water levels. This may be attributed to the accuracy with a time series of tidal elevations forced by the open boundary and the measured tidal level. The simulated tidal current speeds were approximately consistent with the field data (Fig. 5 and Fig. 6). In addition, the simulated direction of tidal currents is consistent with the measured direction of tidal currents as well. The satisfactory validation results demonstrate that the proposed model is capable of simulating the flow in Liao River estuary.

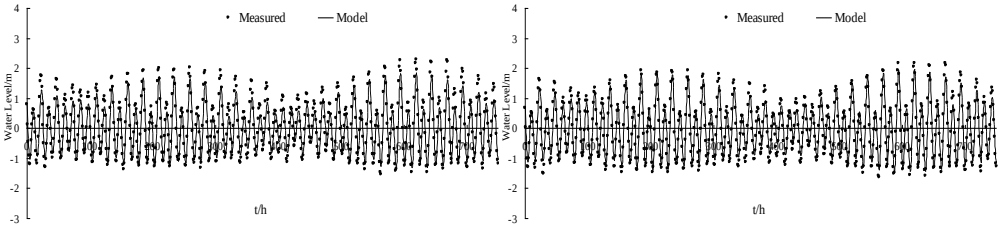

(a) H1 (b) H2

Figure 4. The validation of tidal level at measured stations

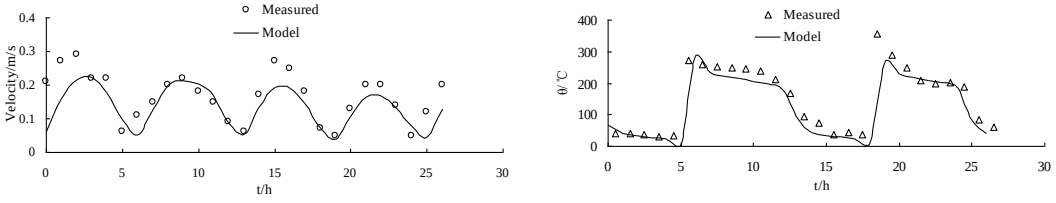

(a) V1

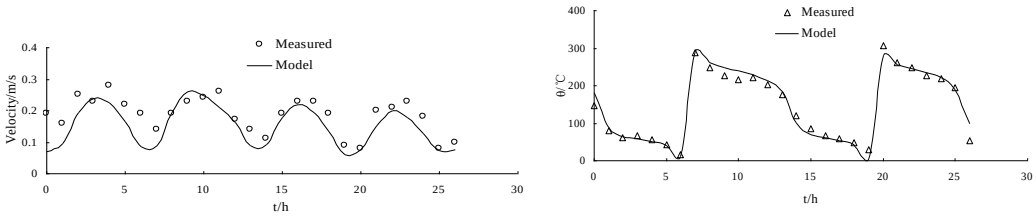

(b) V2

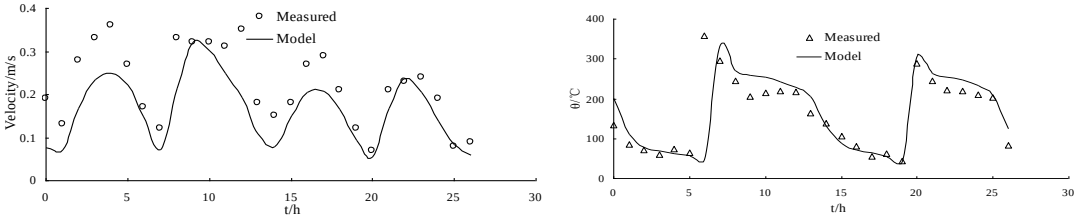

(c) V3

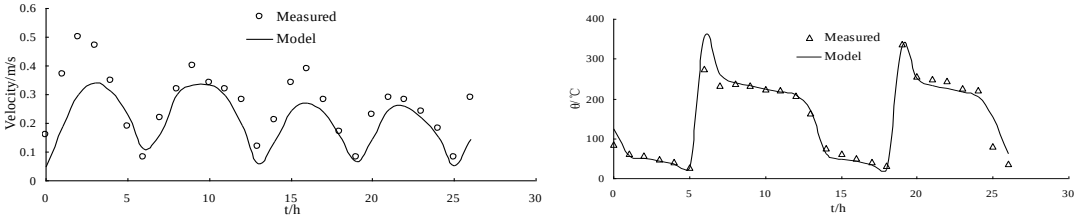

(d) V4

Figure 5. The validation of current speed (left panel) and direction (right panel) at measured stations during neap tide

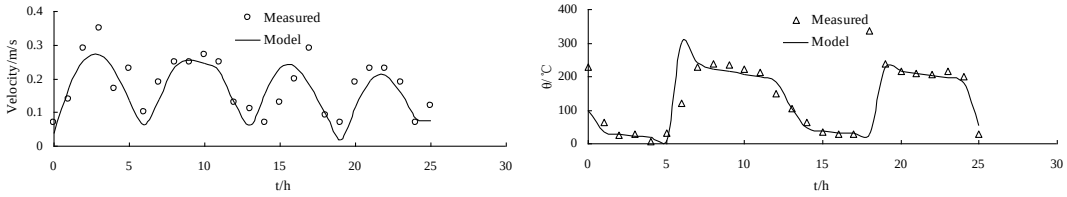

(a) V1

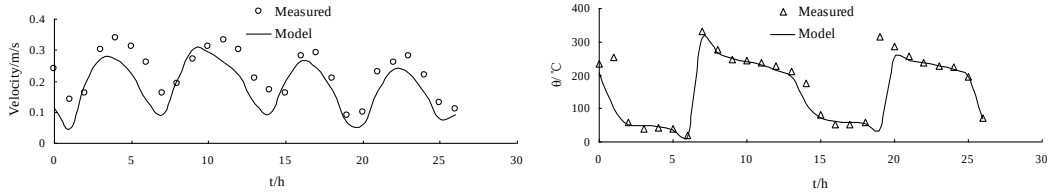

(b) V2

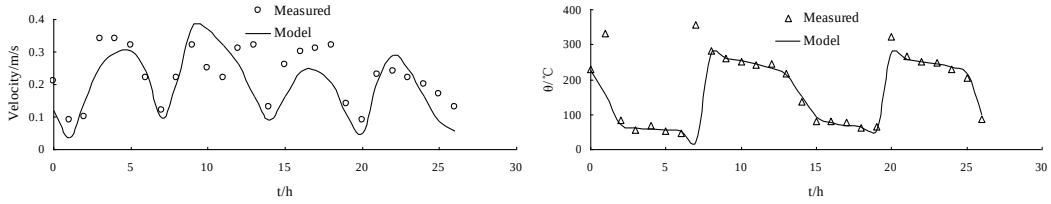

(c) V3

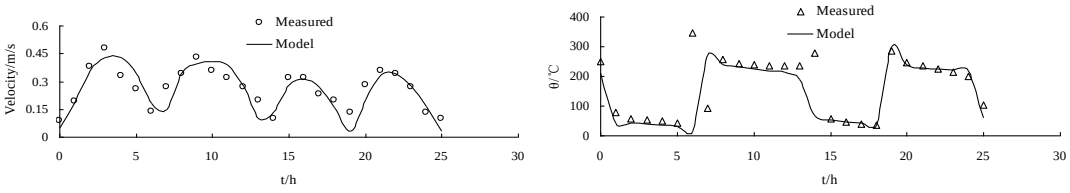

(d) V4

Figure 6. The validation of current speed (left panel) and direction (right panel) at measured stations during spring tide

Fig. 7 and Fig. 8 show the flow field in flood and ebb tide during the neap and spring tide. During the flood tide, as depicted in Fig. 7 (a) and Fig. 8 (a), the general flow of tidal current well offshore is northeastward. The main flow flooding into Liao River divides to go around both sides of Gaizhou shoal. When the flow reaches the east and northeast of the Gaizhou shoal, the flow turns to the northwest, forming a mainstream flow from the outside sea into Liao River. West of Gaizhou shoal, the water flows mainly to the north and the northeast, and is affected by the delta terrain. During the spring tide period, the Gaizhou shoal can be swamped by the tidal currents on both sides because of the high tide level. During the ebb tide period, as depicted in Fig. 7 (b) and Fig. 8 (b), due to the development of many shoals, the current at the mouth of the estuary is divided into many branches. West of the Gaizhou Shoal, the current gradually turns from southwestward to southward. East of the Gaizhou Shoal, the tide current flows directly to southeast and then turns to south. Part of the Gaizhou shoal is high enough to be exposed at the low tide. The results of the salinity validation for V1, V2, V3 and V4 between May 29 and May 30 of 2014 in spring tide are reported in Fig. 9. The model estimates correctly the salinity in the Liao River

estuary. The measured salinities are obtained by Sea-Bird 911 plus Conductivity Temperature Depth (CTD). Overall, the modeled results are acceptable and the model can be used for the following studies.

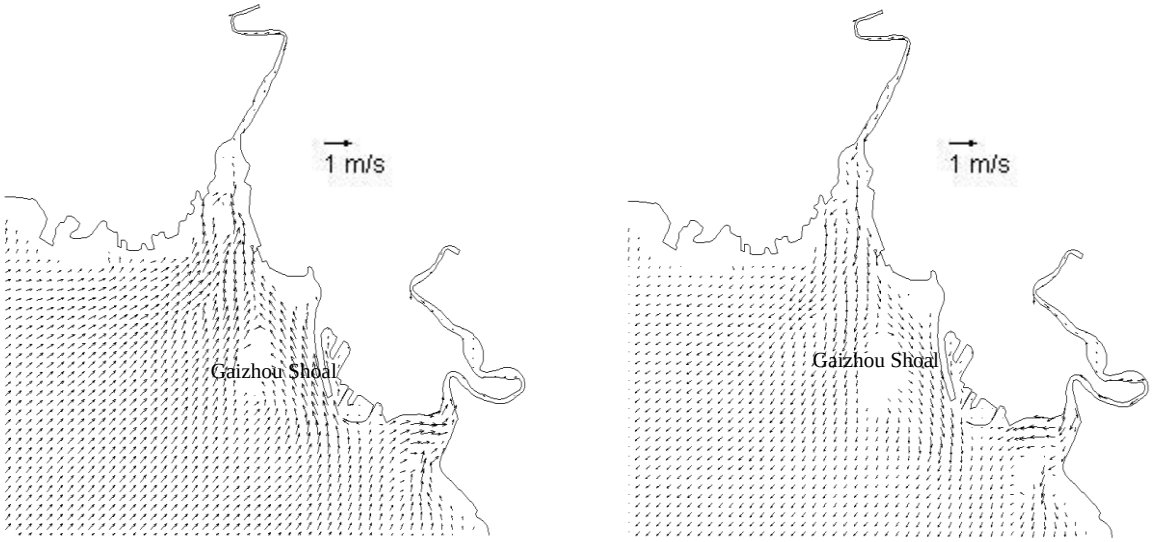

(a) Flood tide (b) Ebb tide

Figure 7. Flow field during neap tide, interpolated to a regular grid for clarity

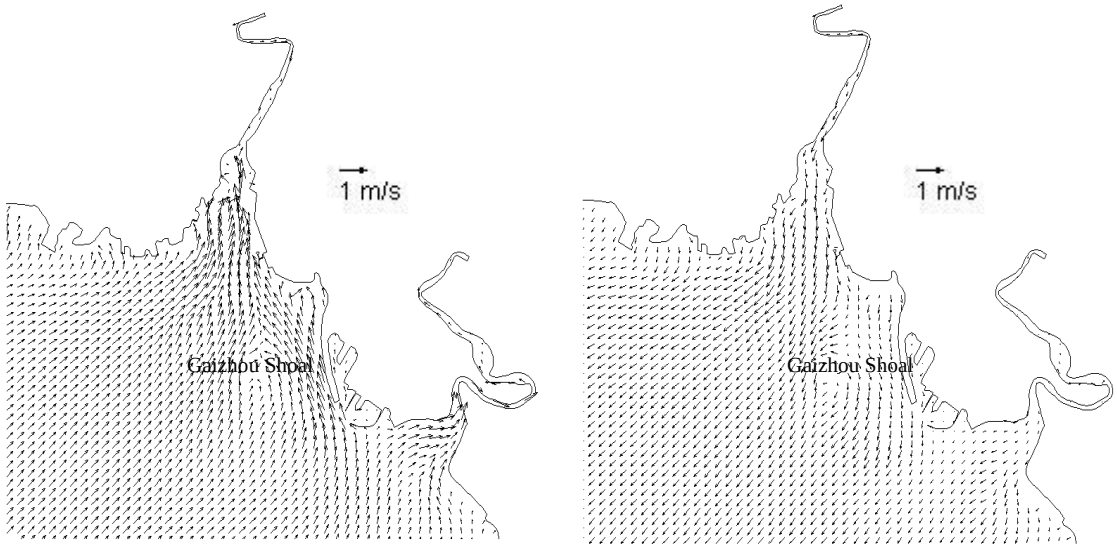

(a) Flood tide (b) Ebb tide

Figure 8. Flow field during spring tide, interpolated to a regular grid for clarity

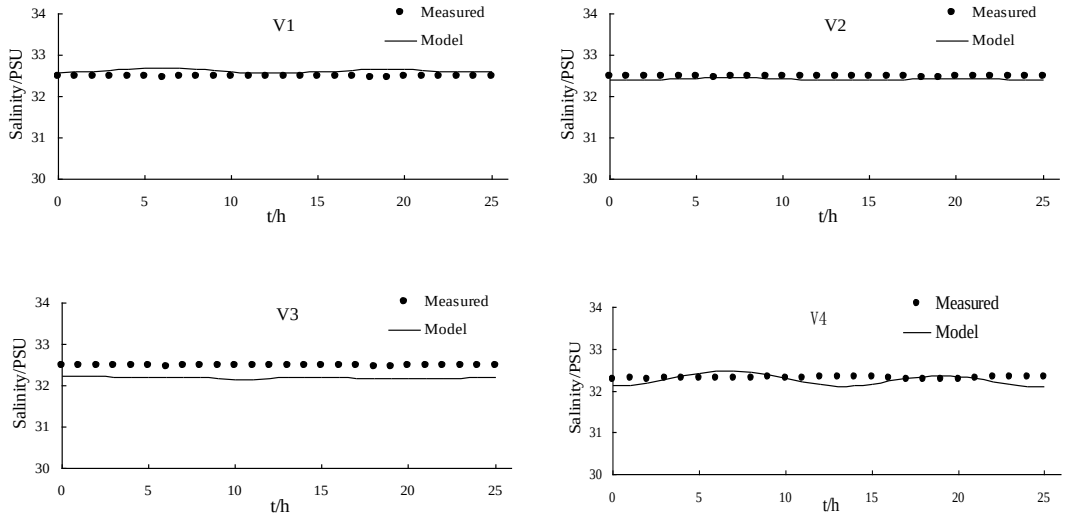

Figure 9. The validation of salinity at measured stations during spring tide

3.3 Hydrodynamics and salinity simulation in Wetland domain

3.3.1 Accessment of wetland information by remote sensing

Remote sensing is an effective and powerful way to monitor vegetation status, growth and biophysical parameters (Hunter et al., 2010; DeFries 2008; Ustin and Gamon 2010) and allow frequent acquisitions for multi temporal studies and reconstruction of historical time series in a cost-effective way (Coppin and Bauer 1994; Munyati 2000). The objective of the present research is to adopt remote sensing to obtain the information of vegetation in wetland of Liao River estuary.

Information on the wetland was acquired on June 3, 2017 from Landsat8 Operational Land Imager (OLI), provided by the USGS (https://glovis.usgs.gov/next/). Resolution of the images is 30m, with orbit number 120/032. The images have undergone radiometric calibration, atmospheric correction and image cutting through ENVI 5.1 software (The Environment for Visualizing Images) before the classification. Firstly, the images were processed via the Radiometric Calibration tool (Zhang et al., 2013), which creates the radiance images. Then, the atmospheric correction of resulting images was carried out

by combining the meta data (solar azimuth angle, image center latitude and longitude, data acquisition time, band gain and band deviation, etc.) through FLAASH (fast line-of-sight atmospheric analysis of spectral hypercubes) Model (Yuan et al., 2009). The focus of this section is on the upper reaches and the Pink Beach, where are vegetation-intensive areas. Therefore, the emphasis on information extraction is water body, shoal and vegetation. The NDVI (normalized difference vegetation index), MNDWI (modified normalized difference water index) and RI (Red index) are used to extract different objects, each index can be extracted for a class of feature information. Firstly, they were calculated based on the reflectance of each band of Landsat8 OLI sensor by using the band functions in ENVI software. Then, different thresholds were set to classify different features. Finally, the decision tree classification (Fig. 10) in ENVI classification tool was executed to realize the extraction of the water body, shoal and vegetation. Vegetation is divided into two categories: *Phragmites communis* and *Suaeda heteroptera* (Fig. 13). The stations of G1, G2, P1, P3 and P5 are presented in Fig.11.

$$\mathrm{MNDWI} = (b3 - b6)/(b3 + b6) \tag{5}$$

$$\mathrm{NDVI} = (b5 - b4)/(b5 + b4) \tag{6}$$

$$RI = (b4 - b3)/(b4 + b3) \tag{7}$$

b3 is the green band reflectance of Landsat8 OLI sensor, b4 is the red band reflectance, b5 is the near infra-red band reflectance, b6 is the middle infra-red band reflectance.

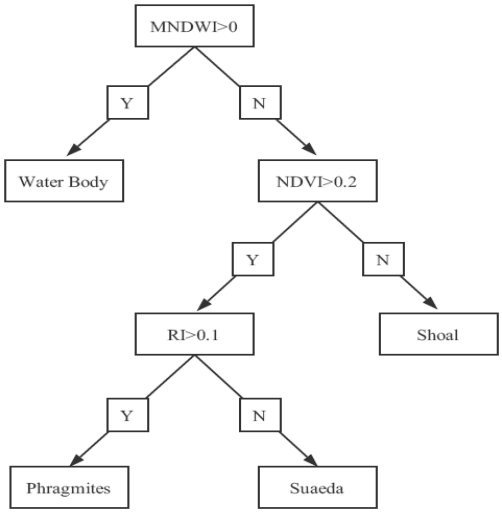

Figure 10. Vegetation classification based on decision tree

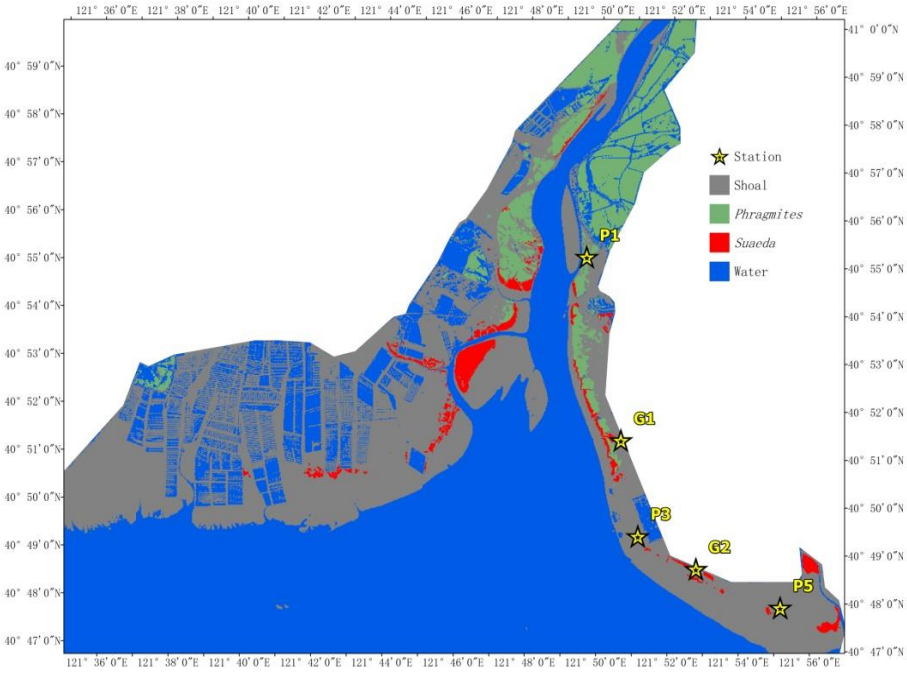

Figure 11. The distribution of aquatic plant and selected stations in Pink Beach

The effect of vegetation on hydrodynamics in areas of wetland in estuary was represented by a varying Manning's coefficient in the bottom friction term. The Manning's coefficient for the vegetation resistance depends on the flow depths, number density and the diameter of the vegetation elements (Zhang et al., 2013). The Manning's coefficient n_v considering vegetation effect is given by

$$n_v = \sqrt{\left(\frac{1}{M}\right)^2 + \frac{C_D m D \min(h, h_v) h^{1/3}}{2g}} \tag{8}$$

where m is the number density (the number of vegetation elements per unit horizontal area), $m = \frac{1}{d_v^2}$, where d_v is the average distance between two adjacent vegetation elements, C_D is the drag coefficient, D is the averaged diameter of the vegetation element, h_v is vegetation height. In vegetated domain, c_f can be expressed $c_f = \frac{g}{(\frac{1}{n_v} h^{1/6})^2}$.

3.3.2 Hydrodynamics and salinity simulation in Wetland domain

The model simulation was conducted to evaluate the estuarine hydrodynamics and salinity transport in the presence of vegetation at the Pink Beach wetland, incorporating realistic vegetation in the model grid. The dominant vegetation at the sites (Fig. 11) is *Phragmites communis* and *Suaeda heteroptera*. The averaged diameters of plants are 0.6 cm and 0.2 cm, respectively; the plant stems are set to 1.5 m and 0.15 m high, respectively. The drag coefficients in the model (C_D) are set to 1.0 and 0.3, respectively (Gu, 2006). The density is set to 65 per square meter for *Phragmites communis* and 200 stems per square meter for *Suaeda heteroptera*, respectively (He et al., 2008). The simulated and measured changes in water depth and salinity concentration at two stations (G1 and G2) are demonstrated in Fig. 12 and Fig. 13. Water depth in the Pink Beach region is correctly modelled, but at G1 upstream of the vegetation zone, this model is in error compared to the observed results. As can be seen from Fig.12, there is asymmetry between flood and ebb tide in the vegetation area. The Liao River estuary has a complex terrain with a large area of tidal flats and shoals, which is one of the causes of the asymmetry of flood

and ebb tide. In addition, there are a large number of *Phragmites communis* and *Suaeda heteroptera* in Pink Beach, the resistance induced by vegetation enhance the tide asymmetry. The model predicts salinity concentration reasonably well compared with the measured data at the Pink Beach. The maximum water depth of G1 is 0.834 m during the spring tide on June 29, the immersion time is 282 minutes; the maximum salinity is 31.02 psu. At G2, the maximum water depth is 0.682 m during the spring tide on July 26 to 27, the immersion time is 184 minutes; the maximum salinity is 34.76 psu. Fig. 14, the velocity of G1 displays double humps, its peak depth-averaged velocity can reach 0.15 ms^{-1}. The measured data and the calculated velocity show good agreement at G1, further confirming the reliability and authenticity of the present simulation. The results of flow structure at Pink Beach in presence and absence of vegetation highlight the relationship between vegetation and currents (Fig.15). From the numerical experiments, it can be seen that the presence of vegetation increases the resistance of the estuary bed and can effectively reduce the flow velocity. This is because when water flows through the vegetation, momentum and energy are lost, the drag exerted by vegetation results in decreased flow speed.

Numerical experiment conducted in the wetland was used to investigate the effect of different plant densities on currents. For the experiments the *Phragmites communis* and the *Suaeda heteroptera* density were doubled to 130 stems/m^2 and 400 stems/m^2, and compared with the currents in the absence of vegetation. As shown in Fig. 16, when there is no vegetation, the flow velocities are larger in wetland. When the density of *Phragmites communis* increased from 65 stems /m^2 to 130 stems /m^2, and the density of *Suaeda heteroptera* increased from 200 stems /m^2 to 400 stems /m^2, the experimental maximum flow velocity in *Suaeda heteroptera* and *Phragmites communis* area decreased by 19% and 6%, respectively. It is clear that the velocity in wetland decreases with higher vegetation densities, there is a negative correlation between currents and vegetation densities.

It is generally acknowledged that the Liao River estuary is a salt-marsh area, the impact of vegetation on water depth and salinity is tested in this paper. Fig. 17 presents the time series of water depth and salinity in vegetated and non-vegetated

experiments at G2. It can be seen that the effects of vegetation on water depth and salinity of wetland domain is not obvious. This is because the tidal wave is long wave, which has no obvious effect on water depth and the salinity of wetland domain.

According to the measured and simulated salinity data of Liao River estuary during the spring tide on July 26 to 27, 2017, five stations were selected from upstream to downstream as shown in Fig.11 in the Pink Beach wetland to analyze the longitudinal distribution of salinity in the tidal cycle under the same runoff conditions. The simulated salinity data for several stations along the Liao River from the entrance are given in Fig. 18, the salinity concentration at P1 upstream is far lower than that of P5 downstream, the salinity concentration increases from upstream to downstream in Liao River. As dilution by fresh water from upstream increases, salinity decreases. During the ebb tide, the negative tide levels occur with the dry domain at locations of G1, G2, P3 and P5, so the salinity concentrations show gaps for this period. The influence of runoff variation on the salinity distribution of G1 and G2 in Pink Beach wetland was analyzed in different runoff conditions 0 m^3s^{-1}, 30 m^3s^{-1}, 101 m^3s^{-1}, 285 m^3s^{-1} and 450 m^3s^{-1}, respectively. As depicted in Fig. 19, the salinity concentration of Pink Beach for 0 m^3s^{-1} is significantly higher than that of other cases. The salinities of G1 and G2 both reach about 32.78 psu in the case of 0 m^3s^{-1}; the salinity of G1 and G2 decreases to about 7.26 and 16.7 psu with 101 m^3s^{-1}; when the runoff is 450 m^3s^{-1}, the salinity concentration of G1 is only 2 psu, and the salinity concentration of G2 is about 5.66 psu. The impact of discharge on salinity distribution in the Liao River estuary is fairly remarkable. During the wet season, due to the higher water discharge, salinity concentrations at G1 and G2 are relatively lower. During the dry season, the flux of fresh water discharged into Pink Beach declines substantially, which leads to enhanced saltwater intrusion. The distributions of salinity at the time of strongest saltwater intrusion with different discharge are presented in Fig. 20. It can be observed that driven by the different runoff, high salinity is mainly concentrated seawards, the lower salinity is in the upper reach of Liao River. Therefore, the larger the river discharge, the stronger is the runoff diluting effect.

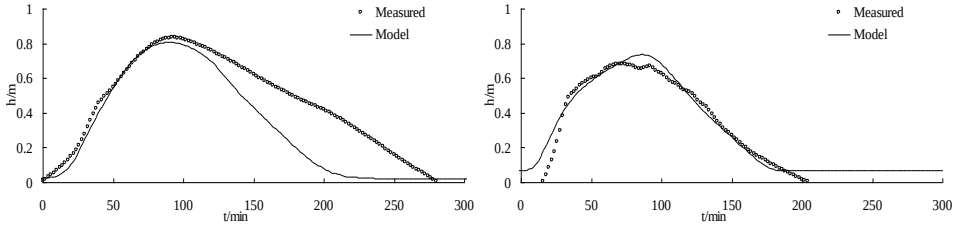

G1 Station G2 Station

Figure 12. Comparison of the simulated and measured water depth at location G1 and G2

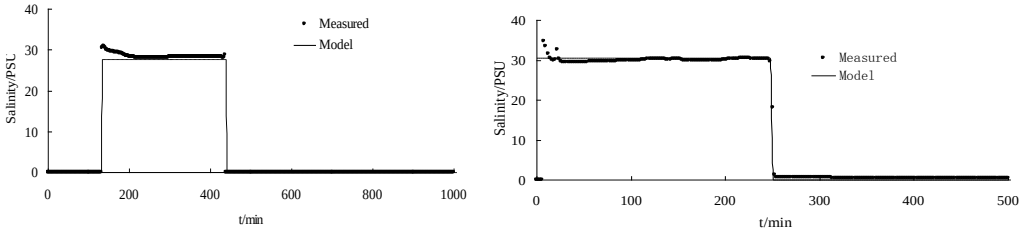

G1 Station G2 Station

Figure 13. Comparison of the simulated and measured salinity concentration at location G1 and G2

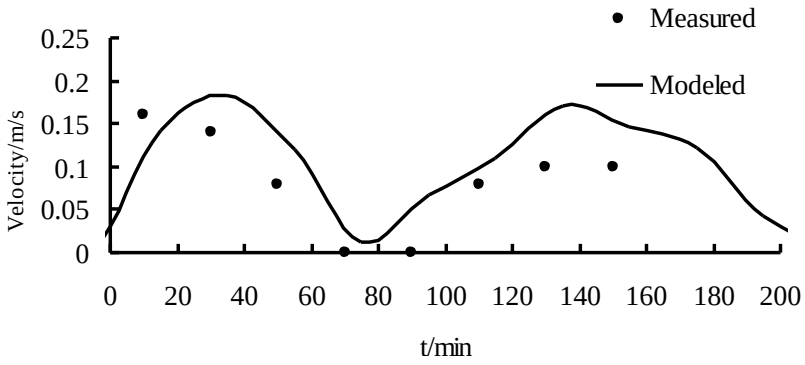

Figure 14. Comparisons of the measured and simulated velocities at location G1

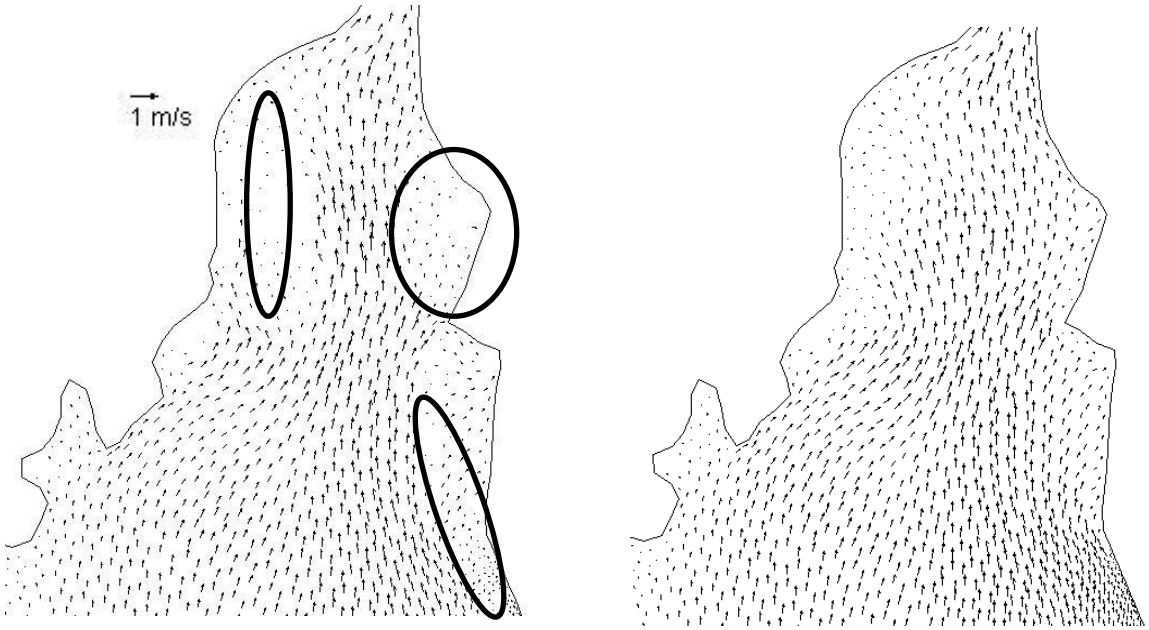

(a) (b)

Figure 15. Flow structure of Pink Beach in vegetated (left panel) and non-vegetated (right panel) area, the black ellipses represent vegetation areas

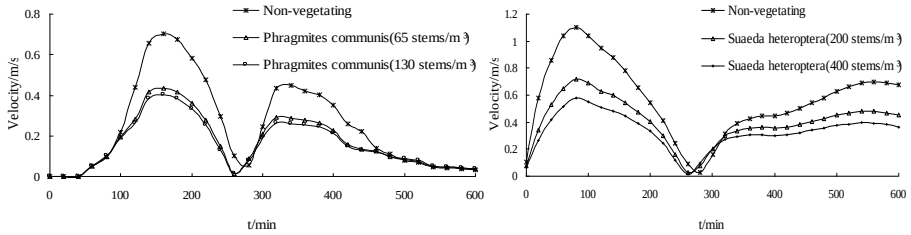

Figure 16. Comparison of the velocities over plant with different plant density in wetland

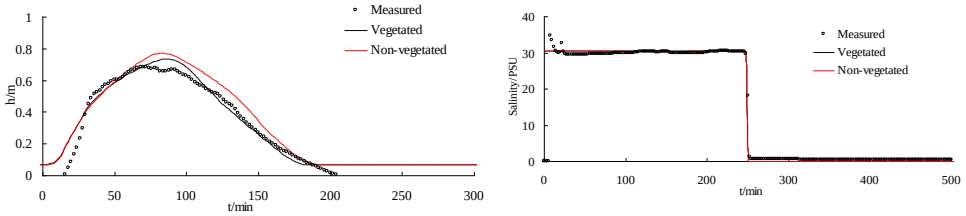

Figure 17. Comparison of the water depth and salinity in vegetated and non-vegetated at location G2

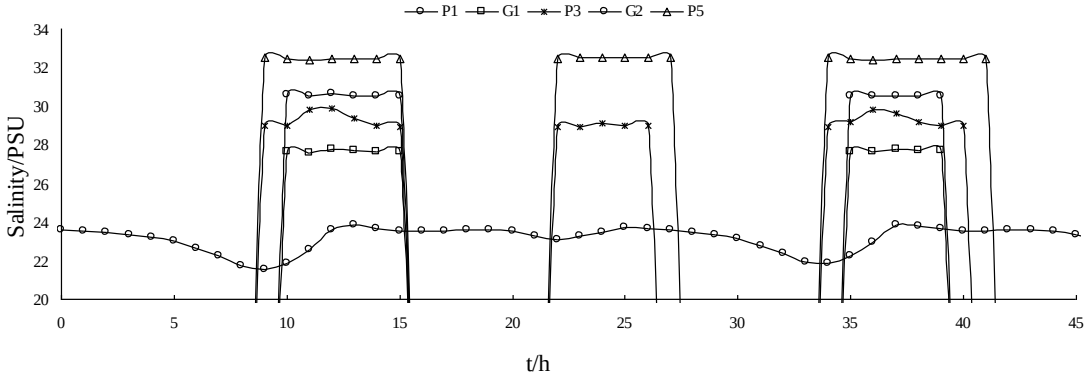

Figure 18. The simulated salinity concentration at five locations

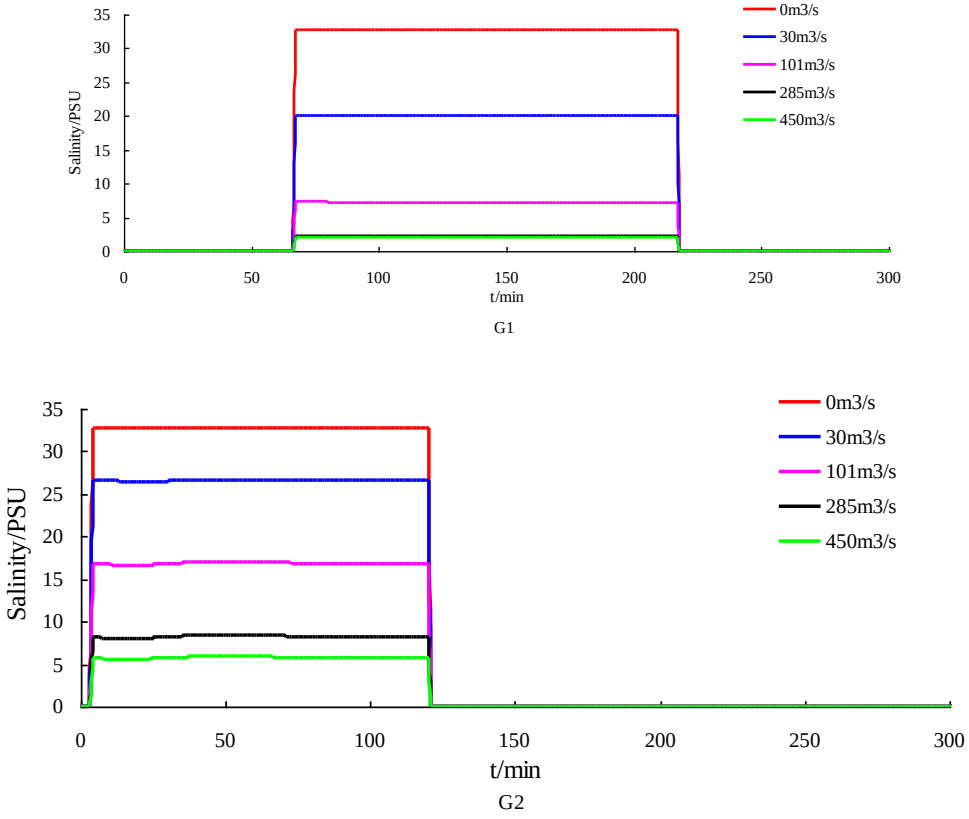

Figure 19. Simulated salinity with different runoff

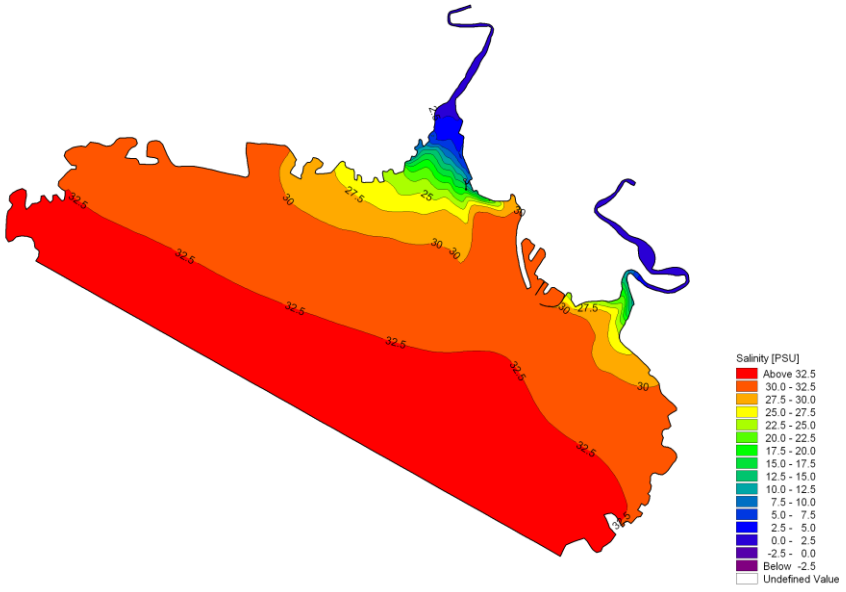

(a) 101m^3/s

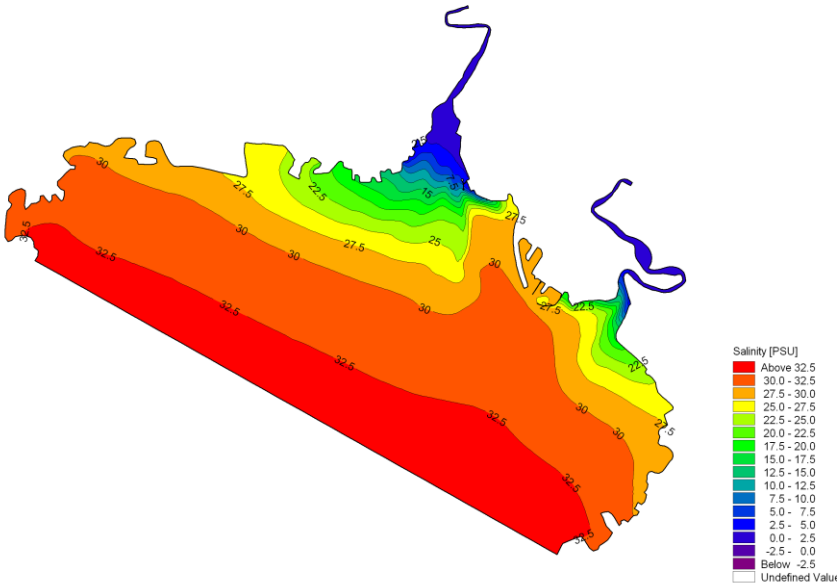

(b) 285m^3/s

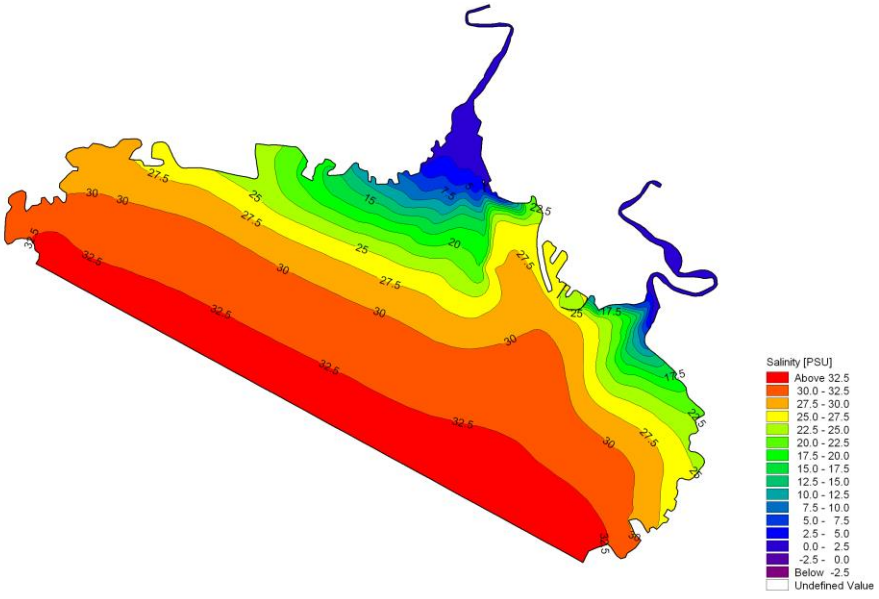

(c) 450m^3/s

Figure 20. Contour maps of salinity for the time of strongest saltwater intrusion with different rates of runoff

4 Discussion

In this study, the MIKE 21 model is used to simulate the hydrodynamic characteristics and salinity transport process in Pink Beach wetlands of Liao River estuary. The model couples the hydrodynamic and salinity modules with salt marsh plant effect. The spatial discretization of the primitive equations is performed using a cell-centered finite volume method in the horizontal plane with an unstructured grid of triangular elements. Landsat images are applied to differentiate the wetland vegetation types in the Liao River estuary. Based on the obvious spectral distinction of vegetations, a decision tree containing a number of decision rules is designed to classify different types of vegetation cover; the Liao River estuary is classified into water body, shoal, and major wetland vegetation types, e.g., *Phragmites communis* and *Suaeda heteroptera*.

The model is tested by simulating the water level, tidal current and salinity concentration in Liao River estuary, and the results are consistent with the measured data. The tidal flats are periodically exposed above the surface of the water in Liao River estuary. Numerical predictions indicate that vegetation imposes significant influence on flow dynamics. The existence of vegetation is associated with lower flow velocities, the vegetation can modify the flow structure owing to energy dissipation induced by vegetation. By analyzing the longitudinal variation of salinity in Pink Beach wetland, we found that salinity gradually increased from upstream to downstream. The effect of runoff on salinity distributions in the Pink Beach is fairly distinct. When the river discharge is low, less freshwater is mixed in and salinity is greater. The results are important to understand the wetland dynamics and salinity transport process, and they contribute to an improved understanding of suitable circumstances for the vegetation growth in Pink Beach as well. More generally, this study can provide an important scientific basis for wetland conservation and restoration.

Acknowledgements. This work was supported by the National Nature Science Foundation of China (51779039), the Wetland Degradation and Ecological Restoration Program of Panjin Pink Beach (PHL-XZ-2017013-002), the Fund of

Liaoning Marine Fishery Department (201725), the Open Fund of the State Key Laboratory of Hydraulics and Mountain River Engineering (SKHL1517).

References

Abu-Bakar A., Ahmadian R., Falconer R. A.: Modelling the transport and decay processes of microbial tracers in a macro-tidal estuary, Water Res., 123: 802–824, 2017.

Andrews, S. W., Gross, E. S., and Hutton, P. H.: Modeling salt intrusion in the San Francisco Estuary prior to anthropogenic influence, Cont Shelf Res., 146: 58–81, 2017.

Barbier, E. B., Koch, E. W., Silliman, B. R., Hacker, S. D., Wolanski, E., Primavera, J., Granek, E. F., Polasky, S., Aswani, S., Cramer, L. A., Stoms, D. M., Kennedy, C. J., Bael, D., Kappel, C.V., Perillo, G. M. E., and Reed, D. J.: Coastal ecosystem-based management with nonlinear ecological functions and values, Sci., 18, 321–323, 2008.

Bouma, T., Vries, M., Low, E., Kusters, L., Herman1, P., Ta ńczos, I., Temmerman, S., Hesselink, A., Meire, P., and Regenmortel, S.: Flow hydrodynamics on a mudflat and in salt marsh vegetation: identifying general relationships for habitat characterizations, Hydrobiologia., 540, 259–274, 2005.

Langevin, C., Swain, E., and Wolfert, M.: Simulation of integrated surface-water/ground-water flow and salinity for a coastal wetland and adjacent estuary, J Hydrol., 314, 212–234, 2005.

Christiansen, T., Wiberg, P. L., and Milligan, T.G.: Flow and sediment transport on a tidal salt marsh surface, Estuarine, Coast. Shelf Sci., 50, 315–331, 2000.

Chow, V. T.: Open-channel hydraulics, New York: McGraw-Hill, 1959.

Cox, B. A.: A review of currently available in-stream water-quality models and their applicability for simulating dissolved oxygen in lowland rivers, Sci Total Environ., 314-316, 335–377, 2003.

Coppin, P., and Bauer, M.: Processing of multitemporal Landsat TM imagery to optimize extraction of forest cover change features, IEEE Geosci Remote S., 32, 918-927, 1994.

DeFries, R.: Terrestrial vegetation in the coupled human-earth system: contributions of remote sensing, Annu. Rev. Environ. Resour., 33, 369-390, 2008.

DHI Software. : Mike 21 flow model: hydrodynamic module scientific documentation, Denmark Hydraulic Institute, 2007.

Feng, K. and Molz, F. J.: A 2-D, diffusion-based, wetland flow model, J Hydrol., 136, 230–250, 1997.

Gu, F. F.: Study on Resistance Coefficient of Reeds and Numerical Simulation of flow in Wetland, PhD thesis, Dalian University of Technology, 2006.

He, Q., Zhou, G., Zhou, L., and Wang, Y.: Aerodynamic parameters and their affecting factors over Panjin reed wetland, Chin. J. Appl. Ecol., 19, 481–486, 2008.

Helmiö, T.: Unsteady 1D flow model of a river with partly vegetated floodplains—application to the Rhine River, Environ Modell Softw., 20, 361–375, 2005.

Hu, K., Chen, Q., and Wang, H.: A numerical study of vegetation impact on reducing storm surge by wetlands in a semi-enclosed estuary, Coast. Eng., 95, 66–76, 2014.

Hunter, P. D., Gilvear, D. J., Tyler, A. N., Willby, N. J., and Kelly, A.: Mapping macrophytic vegetation in shallow lakes using the Compact Airbone Spectrographic Imager (CASI), Aquat Conserv., 20, 717–727, 2010.

Ikeda, S. and Kanazawa, M.: Three-dimensional organized vortices above flexible water plants, J Hydraul Eng., 122, 634–640, 1996.

Jiang, T. T., Pan, J. F., Pu, X. M., Wang, B., and Pan, J. J: Current status of coastal wetlands in China: Degradation, restoration, and future management, Estuarine, Coast. Shelf Sci., 164, 265–275, 2015.

Lapetina, A. and Sheng, Y. P.: Three-Dimensional Modeling of Storm Surge and Inundation Including the Effects of Coastal Vegetation, Estuar Coast., 37(4): 1028 – 1040, 2014.

Li, H., Ye, S., Ye, J., Fan, J., Gao, M., and Guo, H.: Baseline survey of sediments and marine organisms in Liaohe Estuary: Heavy metals, polychlorinated biphenyls and organochlorine pesticides, Mar. Pollut. Bull., 114, 555-563, 2017.

Li, Y. and Z, M.: Experimental studies of hydrodynamics in vegetated river flows—Vertical profiles of velocity, shear velocity and Manning roughness, J Hydrodyna., 19, 515-519, 2004.

Munyati, C.: Wetland change detection on the Kafue Flats, Zambia, by classification of a multitemporal remote sensing image dataset, Int J Remote Sens., 21, 1787-1806, 2000.

Padman, L.: Tide Model Driver (TMD) Manual, Earth & Space Research, 2005.

Ree, W.: Retardation Coefficients for Row Crops in Diversion Terraces, Transactions of the American Society of Agricultural Engineers., 78-80, 1958.

Shi, Z.: A flume study on mean velocity profiles of flow in a coastal saltmarsh canopy, Ocean Eng., 19, 51-59, 2001.

Stark, J., Meire, P., and Temmerman, S.: Changing tidal hydrodynamics during different stages of eco-geomorphological development of a tidal marsh: A numerical modeling study, Estuarine, Coast. Shelf Sci., 188, 56-58, 2017.

Su, Y. T., Hock, L. K., Donald, L. D., and Mike, T.: Interaction between salinity intrusion and vegetation succession: A modeling approach, Theor Appl Mech., 3(3): 032–001, 2013.

Sun, D. T., Wan, Y. S., and Qiu, C.: Three-dimensional model evaluation of physical alteration of the Caloosahatchee River and Estuary: Impact on salt transport, Estuarine, Coast. Shelf Sci., 173: 16–25, 2016.

Temmerman, S., Meire, P., Bouma, T., Herman, P., Ysebaert, T., and De, H.: Ecosystem-based coastal defence in the face of global change, Nature., 504, 79–83, 2013.

Ustin, S. and Gamon, J.: Remote sensing of plan functional types, New Phytol., 186, 795-816, 2010.

Wang, J., Ye, S., Edward, A. L., Yuan, H., Ding, X., and Zhao, G.: Surface sediment properties and heavy metal pollution assessment in the Shallow Sea Wetland of the Liaodong Bay, China, Mar. Pollut. Bull., 120, 347-354, 2017.

Wang, Q. G., Li, S. B., Jia, P., Qi, C. J., and Ding, F.: A review of surface water quality models, Sci. World J., 2013.

Wilson, C. A. M. E., Yagci, O., Rauch, H. P., and Olsen, N. R. B.: 3D numerical modelling of a willow vegetated river/floodplain system, J. Hydrol., 327, 13–21, 2006.

William, R.: Computational hydraulics: Elements of the Theory of Free Surface Flows, Coast. Eng., 3, 278, 1979-1980.

Yuan, J.G., Niu,Z., Wang, X.P.: Atmospheric correction of hyperion hyperspectral image based on FLAASH. Spectrosc. Spect. Anal., 29, 1181-1185, 2009.

Zhang, M. L., Li, C. W., and Shen, Y. M.: Depth-averaged modeling of free surface flows in open channels with emerged and submerged vegetation, Appl Math Model., 37, 540-553, 2013.

Zhang, X. L., Zhang, Z. H., Gu, D. Q., Xu, Z. J., and Ye, S.: Research on evolution of coastal wetlands in Liaohe River Delta, Ecology and Environmental Sciences., 18, 1002-1009, 2009 (In Chinese).

Zhang, S. W., Yan, F. Q., Yu, L. X., Bu, K., Yang, J. C., and Chang, L. P.: Application of Remote Sensing Technology to Wetland Research, Scientia Geographica Sinica., 33, 1406-1410, 2013 (In Chinese).